Two-Dimensional Metal Dichalcogenides and Oxides for Hydrogen Evolution: A Computational Screening Approach

ARTICLE *in* JOURNAL OF PHYSICAL CHEMISTRY LETTERS · APRIL 2015

Impact Factor: 7.46 · DOI: 10.1021/acs.jpclett.5b00353

4 AUTHORS, INCLUDING:

Mohnish Pandey
Technical University of Denmark
10 PUBLICATIONS **16** CITATIONS
SEE PROFILE

Aleksandra Vojvodic
SLAC National Accelerator Laboratory/Stanf…
52 PUBLICATIONS **792** CITATIONS
SEE PROFILE

Kristian Sommer Thygesen
Technical University of Denmark
145 PUBLICATIONS **4,293** CITATIONS
SEE PROFILE

THE JOURNAL OF PHYSICAL CHEMISTRY Letters

Letter

pubs.acs.org/JPCL

Two-Dimensional Metal Dichalcogenides and Oxides for Hydrogen Evolution: A Computational Screening Approach

Mohnish Pandey,[†] Aleksandra Vojvodic,[‡] Kristian S. Thygesen,[†,§] and Karsten W. Jacobsen*[,†]

[†]Center for Atomic-Scale Materials Design, Department of Physics, Technical University of Denmark, DK-2800 Kongens Lyngby, Denmark

[‡]SUNCAT Center for Interface Science and Catalysis, SLAC National Accelerator Laboratory, 2575 Sand Hill Road, Menlo Park, California 94025, United States

[§]Center for Nanostructured Graphene (CNG), Department of Physics, Technical University of Denmark, DK-2800 Kongens Lyngby, Denmark

Supporting Information

ABSTRACT: We explore the possibilities of hydrogen evolution by basal planes of 2D metal dichalcogenides and oxides in the 2H and 1T class of structures using the hydrogen binding energy as a computational activity descriptor. For some groups of systems like the Ti, Zr, and Hf dichalcogenides the hydrogen bonding to the 2H structure is stronger than that to the 1T structure, while for the Cr, Mo, and W dichalcogenides the behavior is opposite. This is rationalized by investigating shifts in the chalcogenide p levels comparing the two structures. We find that usually for a given material only at most one of the two phases will be active for the hydrogen evolution reaction; however, in most cases the two phases are very close in formation energy, opening up the possibility for stabilizing the active phase. The study points to many new possible 2D HER materials beyond the few that are already known.

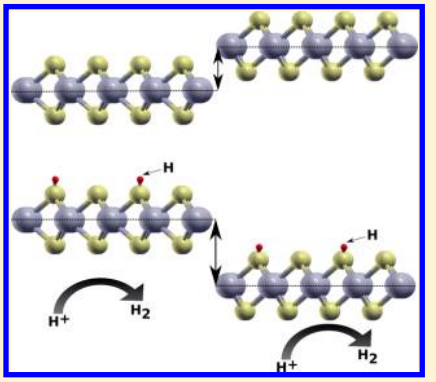

Hydrogen holds a crucial place in many chemical syntheses and in energy production;[1,2] however, an economical process for hydrogen production has not been fully realized yet. One of the main challenges lies in finding a cheap catalyst that can evolve hydrogen efficiently. Platinum, which is known to be one of the best catalysts for hydrogen evolution, is prohibitively expensive, thus precluding it to be used on large scales. Several other metals, metal surface alloys and metal oxides, have been studied for the same reaction, but unfortunately most of these are not both efficient and cheap at the same time.[3−5] Only recently a few and interesting candidates have been identified for hydrogen evolution reaction (HER), for example, Ni_2P.[6,7]

Recent promising experiments on 2D metal sulfides have opened up a new class of materials that could contain promising candidates for HER.[8−12] The 2D nature of these materials gives additional flexibility of nanostructuring and manipulating the structures, which is otherwise challenging in the 3D bulk form. For example, MoS_2 exists in both 2H and 1T phases in monolayer form, whereas the 1T phase is thermodynamically unfavorable in the bulk.[13] Despite the fact that the 2H-MoS_2 is one of the most studied 2D sulfides for HER, it has active sites on the edges only,[14,15] and the limited activity is ascribed to the inability of the 2H-MoS_2 basal plane to adsorb hydrogen.[10] The above limitation has been overcome by contemporary experiments on 1T-MoS_2 and WS_2, in which the entire sheet has been found to be catalytically active for HER.[8−10] The unusual difference between the 2H and 1T phases thus expands the material space to more structures that might be relevant for the given application.

In the present work, we explore the HER activity of the basal planes of 100 dichalcogenides and oxides (MX_2) in both the 2H and 1T class of structures using the free energy of hydrogen adsorption as a descriptor for the activity of the material.[3,16] Rather than assuming the existence of perfectly symmetrical 2H and 1T structures, we carefully look for deviations of the atomic structure from the perfectly symmetric 2H and 1T phases and choose the structure with minimum energy. (We continue using the terminology 2H and 1T for distorted structures as well to avoid cluttering of notations.) We choose 'M' from a set of 25 elements (shown in the ordinate of Figure 2) and 'X' from a set of 4 (shown in the abscissa of Figure 2) elements (chalcogens and oxygen). We find a significant difference in the hydrogen adsorption energy of the 2H and 1T phases of a given compound; on the other hand, the 2H and 1T phases show similar thermodynamic stability, thus making it possible to stabilize the structure showing activity toward HER despite the fact that it is not the most stable structure. To find a correlation between the adsorption energies and the nature of metal atoms, we group the compounds based on the position of the metal atoms in the periodic table. For the groups showing apparent

Received: February 17, 2015
Accepted: April 10, 2015

DOI: 10.1021/acs.jpclett.5b00353
J. Phys. Chem. Lett. 2015, 6, 1577−1585

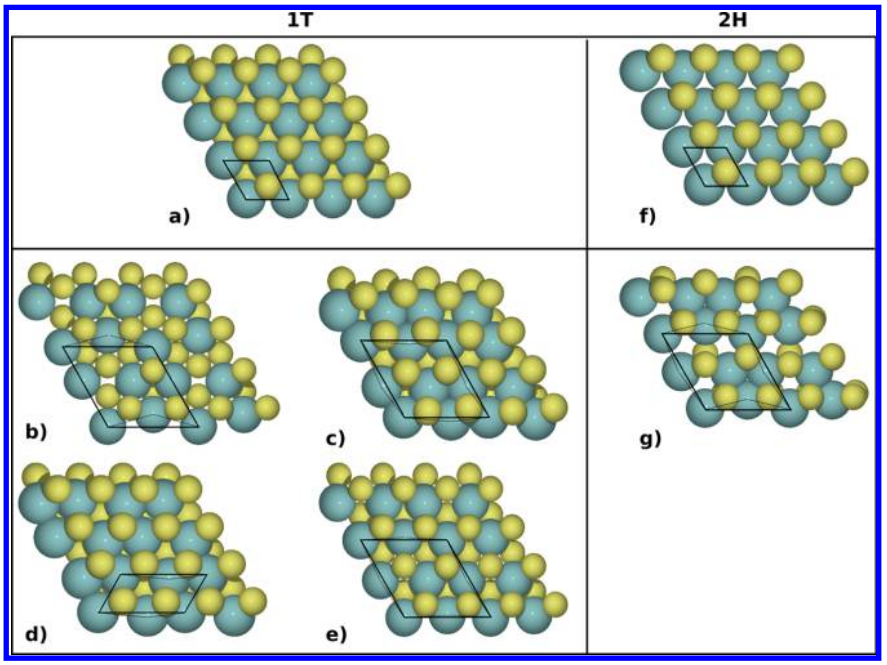

Figure 1. (a) Top view of a 1T monolayer ($P\bar{3}2/m1$ space group). (b) Monolayer with distortions belonging to the 1T class and $P1$ spacegroup with unit cell size 2 × 2. (c) Monolayer with distortions belonging to the 1T class and $P\bar{1}$ spacegroup with unit cell size 2 × 2. (d) Monolayer with distortions belonging to the 1T class and $P1$ spacegroup with unit cell size 2 × 1. (e) Monolayer with distortions belonging to the 1T class and $P3m1$ spacegroup with unit cell size 2 × 2. (f) Top-view of a 2H monolayer ($P\bar{6}m2$ space group). (g) Monolayer with distortions belonging to the 2H class and $P1$ spacegroup with unicell size 2 × 2. Unit cells have been drawn (black solid lines) to show the size of the unit cell, and a few selected bonds (black broken lines) between metal atoms have been shown to highlight the difference between different structures.

difference of the 2H and 1T phases for hydrogen adsorption, we show that the relative position of the p level of 'X' with respect to the Fermi level plays a decisive role for hydrogen adsorption. On the basis of the descriptor employed to screen the materials for HER, we point to many new possible 2D HER materials beyond the few that are already known.

In the present work, we use GPAW,[17] an electronic structure code based on the projector-augmented wave (PAW)[18] formalism. The PBE[19] functional is used for the calculation of lattice constants, and the calculated lattice constants have been used throughout the work. Structures showing distortions have been reoptimized, and the recalculated lattice constants are used. We calculate the heat of formation using the fitted elemental reference phase energies (FERE) scheme employed over the PBE calculated energies, as proposed by Stevanovic et al.[20] A grid spacing of 0.18 Å is used to expand the wave functions in real space, and a Fermi−Dirac smearing of 0.05 eV is employed to accelerate the convergence. The Brillouin zone for the smallest unit cell (1 × 1) is sampled using a Monkhorst−Pack[21] scheme with a k-point mesh of 18 × 18 × 1, and for 2 × 2 unit cells, we use a 9 × 9 × 1 k-point grid. All optimizations are carried out using a Quasi-Newton algorithm, and the forces are converged down to 0.05 eV/Å for all relaxations. Spin-polarized calculations are performed for the calculation of lattice constants as well as for the adsorption energies. Adsorption energies are calculated using the BEEF-vdW functional.[22] Uncertainties in adsorption energies are explicitly calculated using the ensemble of functionals proposed in ref 22. The calculated uncertainties are used to estimate the probability that a given material will have the free-energy descriptor for HER lying within a given range. The calculated probabilities help to rank the different materials based on their suitability[23] for HER. We add several corrections to the calculated total energy differences to estimate the adsorption free energy. The zero point energy corrections to the energies of all systems are to a first order approximation taken to be the same as the ones calculated for the 1T-MoS_2 monolayer structure. We get the zero-point correction of the adsorbed hydrogen as 0.39 eV at the standard state. We ignore the entropic corrections for the adsorbed state while calculating the total correction as in ref 15. The zero-point energy of the H_2 molecule has been taken from the ref 24 and is found to be 0.54 eV. The entropic correction of 0.40 eV from the gas-phase H_2 is taken from ref 25. By taking the difference of the corrections in the gas phase and the adsorbed state, ΔZPE comes out as 0.12 eV and $-T\Delta S$ comes out as 0.20 eV; therefore, $\Delta ZPE - T\Delta S$ comes out to be 0.32 eV.

The current work focuses on the 2H and 1T structures and their distorted derivatives of 2D metal dichalcogenides and oxides some of which have been realized in recent experiments.[10−12] The structural difference between the 1T and 2H phases originates from the difference in coordination environment around the metal atom. The 2H phase of MX_2 has a trigonal prismatic structure with 'M' at the center of the prism and 'X' at the vertices, where the 1T phase has an octahedral coordinated structure with 'M' at the center of the octahedron and 'X' at the vertices. Figure 1a,f shows the top view of the 2H and 1T structure, respectively. Figure 1b−e,g represents distorted derivatives of the 2H and 1T structures, which will be discussed later. The significant difference in atomic structure of the two phases might lead to differences in their thermodynamic and electronic properties. The difference in thermodynamic properties will directly influence the relative stability of the two phases, whereas different electronic properties will have an effect on the chemical reactivity. To detect the distortions, if any, in the 2H and 1T structures, we follow the steps: (1) Adsorb the hydrogen in the 2 × 2 unit cell to break the symmetry of the structure and allow the structure

DOI: 10.1021/acs.jpclett.5b00353
J. Phys. Chem. Lett. 2015, 6, 1577−1585

to relax. (2) Remove the hydrogen from the structure obtained from step 1 and relax the structure. (3) If the structure obtained after step 2 is the same as the perfectly symmetric structure, then there are no distortions present or else the structure is distorted. (4) Cases may exist in which step 2 leads to local minima in new structures; therefore, one has to compare the energy obtained after step 2 and the energy of the perfectly symmetric structure and choose the one with lower energy.

Following the steps previously outlined, the distortions present under HER conditions can most likely be obtained. Similar distortions in MoS_2 have been explored by Kan et al.,[26] but we see a wider range of distortions. Therefore, instead of using their terminology, we categorize the distortions in a more general way based on the space group and the size of the unit cell.

Figure 2a,b shows the calculated standard heats of formation of the 2D MX_2 compounds in the 2H and 1T phases. In

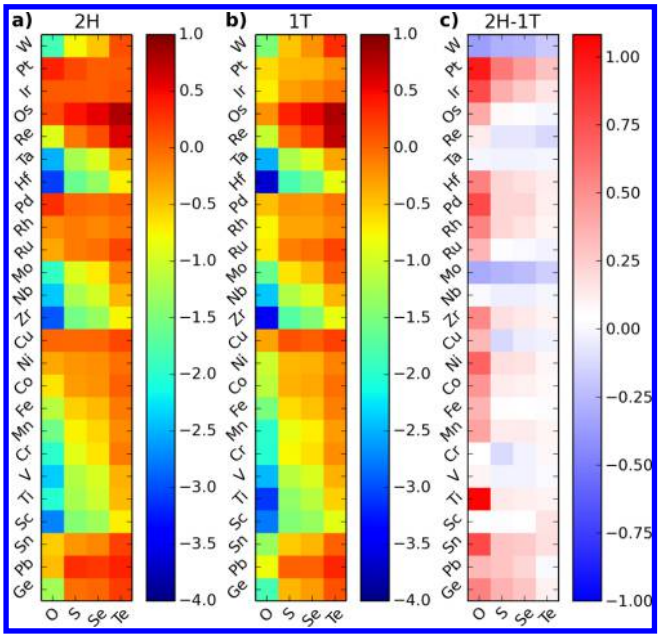

Figure 2. (a,b) Heatmap of standard heat of formation (in eV/atom) of compounds in undistorted 2H and 1T structures, respectively. (c) Difference in enthalpies between the 2H and 1T structures (in eV/atom) of different compounds. Each compound is represented by a square, and the constituent elements are represented by the corresponding ordinate and abscissa of the square. The difference in energies is in eV/atom.

calculating the standard heat of formation, we neglect any zero-point or entropic correction. As can be seen from the Figure the region of stable compounds is very similar in the two structures. With very few exceptions, the compound that is stable (unstable) in one structure exhibits stability (instability) in the other structure as well. Figure 2c shows the difference in enthalpies of the different compounds by which we can estimate the extent to which the two phases differ thermodynamically. The obtained trend in the relative stability of the 2H and 1T phases agrees well with the calculations of Ataca et al.[27] We see that for most of the compounds the energy difference between the 2H and the 1T phase is smaller than ~0.4 eV/atom. Recent experiments on MoS_2[10] and WS_2[8] show that the distorted 1T phase despite being energetically higher than the 2H phase by ~0.3 eV/atom can be stabilized. These experiments thus suggest that the metastable phase of a 2D MX_2 compound with a positive heat of formation as high as ~0.3 eV/atom relative to the stable phase can be synthesized and stabilized under normal conditions using suitable synthetic routes.[28] Thus, the generally small energy differences shown in Figure 2c indicate that the atomic structure of 2D MX_2 can be tuned, if required, for the application in hand. Therefore, we explore both the 2H and 1T class of structures of MX_2 to find suitable materials for HER.

Figure 3a,b shows the energy of distorted structures with respect to perfectly symmetric 2H and 1T structures,

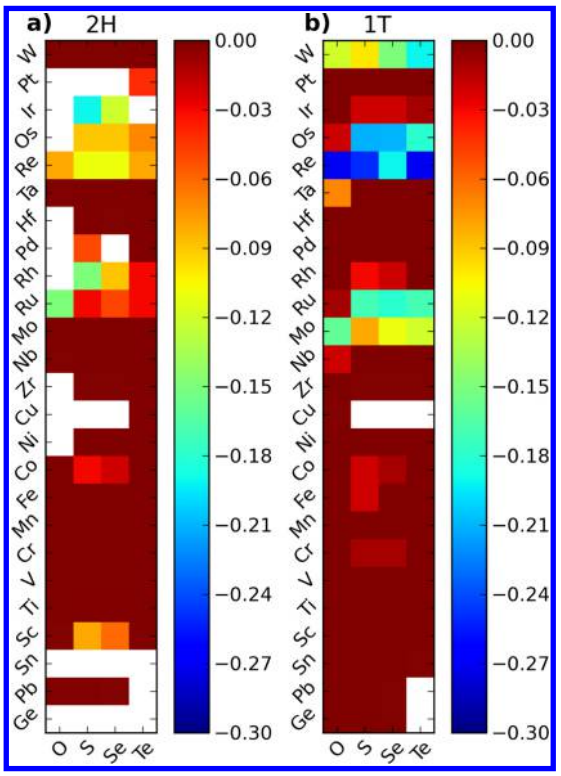

Figure 3. (a,b) Energy of the distorted structures (eV/atom) with respect to the perfectly symmetrical 2H and 1T structures, respectively. The white squares denote massive reconstruction upon relaxation, thus leading to structures not belonging to the 2H and 1T class of structures.

respectively. The white squares denote massive reconstruction upon relaxation, thus leading to structures neither belonging to the 2H or 1T class of structures. We do not investigate these systems any further. Upon analyzing the nature of reconstructions in the more moderately distorted structures, it turns out that the distortions occurring in the 1T structure can be categorized in four different symmetry groups, whereas the distortions in the 2H structure can be captured by only one group. Starting with the structures with slightly displaced atoms from their ideal positions in the perfect 2H and 1T structures, that is, without symmetries in a 2 × 2 unit cell, upon relaxation, some compounds in 1T structure gain symmetry in such a way that all of the symmetry operations can be captured in a 2 × 1 unit cell, thus leading to reduction in the size of unit cell. This is not the case for any of the 2H structures. Therefore, we categorize the distorted structures based on the space groups and the unit cell size using the tool described in ref 29. Table 1 shows the categorization of the distortions based on the space group and the size of the reduced unit cell. The forces cannot be brought down to exactly zero during the optimization

DOI: 10.1021/acs.jpclett.5b00353
J. Phys. Chem. Lett. 2015, 6, 1577−1585

Table 1. Categorization of Different Compounds Based on the Deviation of Their Structures from Perfect 2H or 1T Structures and the Size of the Unit Cell[a]

class	MX_2	group	unit cell	class	MX_2	group	unit cell
2H	CoS_2	*P*1	2 × 2	2H	$CoSe_2$	*P*1	2 × 2
2H	IrS_2	*P*1	2 × 2	2H	OsS_2	*P*1	2 × 2
2H	$OsSe_2$	*P*1	2 × 2	2H	PdS_2	*P*1	2 × 2
2H	$PdSe_2$	*P*1	2 × 2	2H	$PdTe_2$	*P*1	2 × 2
2H	ReO_2	*P*1	2 × 2	2H	ReS_2	*P*1	2 × 2
2H	$ReSe_2$	*P*1	2 × 2	2H	RhS_2	*P*1	2 × 2
2H	$RhSe_2$	*P*1	2 × 2	2H	$RhTe_2$	*P*1	2 × 2
2H	RuO_2	*P*1	2 × 2	2H	RuS_2	*P*1	2 × 2
2H	$RuSe_2$	*P*1	2 × 2	2H	ScS_2	*P*1	2 × 2
2H	$ScSe_2$	*P*1	2 × 2				
1T	CoS_2	*P*1	2 × 2	1T	CrS_2	*P*1	2 × 2
1T	$CrSe_2$	*P*1	2 × 2	1T	FeS_2	*P*1	2 × 2
1T	IrS_2	*P*1	2 × 2	1T	$IrSe_2$	*P*1	2 × 2
1T	ReO_2	*P*1	2 × 2	1T	$ReTe_2$	*P*1	2 × 2
1T	RhS_2	*P*1	2 × 2	1T	RuS_2	*P*1	2 × 2
1T	$RuTe_2$	*P*1	2 × 2	1T	MoO_2	*P*1	2 × 1
1T	MoS_2	*P*1	2 × 1	1T	$MoSe_2$	*P*1	2 × 1
1T	$MoTe_2$	*P*1	2 × 1	1T	OsS_2	*P*1	2 × 1
1T	$OsSe_2$	*P*1	2 × 1	1T	$OsTe_2$	*P*1	2 × 1
1T	WS_2	*P*1	2 × 1	1T	WSe_2	*P*1	2 × 1
1T	WTe_2	*P*1	2 × 1	1T	ReS_2	$P\bar{1}$	2 × 2
1T	$ReSe_2$	$P\bar{1}$	2 × 2	1T	$RuSe_2$	$P\bar{1}$	2 × 2
1T	TaO_2	$P\bar{1}$	2 × 2	1T	$CoSe_2$	*P*3*m*1	2 × 2
1T	$IrTe_2$	*P*3*m*1	2 × 2	1T	NbO_2	*P*3*m*1	2 × 2
1T	OsO_2	*P*3*m*1	2 × 2	1T	$RhSe_2$	*P*3*m*1	2 × 2
1T	RuO_2	*P*3*m*1	2 × 2	1T	WO_2	*P*3*m*1	2 × 2

[a]The class represents the type of undistorted structure to which the compound belongs, the group represents the space group of the distorted structure as per Herman−Maugin notation, and the unit cell represents the size of the reduced unit cell with respect to the 1 × 1 unit cell of the perfect 2H or 1T structures.

process; therefore, to overcome inaccuracies in the forces, we employ a cutoff of 0.05 Å on the rotations/translations to identify the symmetry operations. For six structures where the difference in energy of the distorted structure and the perfectly symmetrical structure is <0.01 eV per atom, we categorize them into the symmetrical structure for the previously mentioned reason. We find that for all of the distorted structures in the 2H class, the type of distortion is similar to the one shown in Figure 1g. Therefore, we categorize them in the same class as those that have the unit cell size of 2 × 2 and the space group *P*1. Figure 1b−e shows the four different types of distortions observed in the 1T structure. There are subtle differences in all of these four groups. Panel b does not have any symmetry and thus belongs to the *P*1 group, panel c shows the distortions similar to panel b but has an inversion symmetry and thus belongs to $P\bar{1}$ as also observed by Tongay et al. for ReS_2.[30] The distortions in panel d are such that the structure forms stripes with periodicity of one unit cell, resulting in a unit cell size of 2 × 1. Panel e has the least distortion and inherits most of the symmetry operations from the symmetric 1T structure and belongs to the *P*3*m*1 space group.

Additionally, as previously mentioned, discarding distorted phases that differ in energy from the perfectly symmetric structures by <0.01 eV per atom might result in missing some of the charge density wave (CDW) phases, for example, in TiS_2.[31,32] In the case of TiS_2 we found that for a 12 atom unit cell (2 × 2 unit cell) the distorted and the perfectly symmetric structure differ by only ∼0.04 eV (∼0.004 eV per atom). It turns out that due to similar energy differences the CDW phases of other compounds, for example, TaS_2, are all discarded due to the previously mentioned reason. Discarding the CDW phases does not affect our results for the HER, which is dependent only on the energy differences, which are very small in the previously mentioned cases.

In previous works the strength of hydrogen binding on a catalyst surface has been used as a descriptor for the ability to

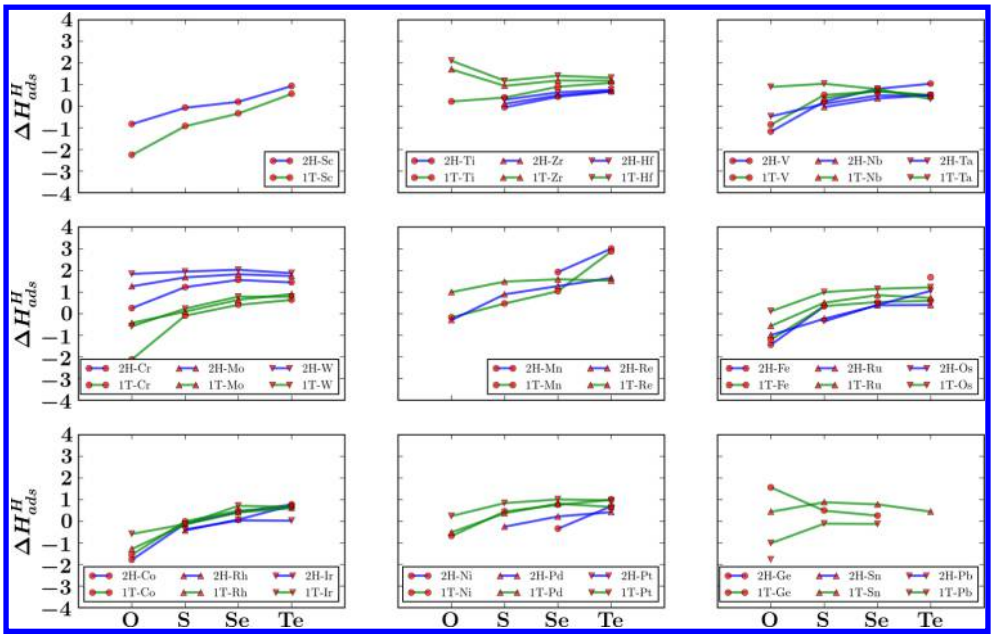

Figure 4. Adsorption energies of the individual groups of compounds. The grouping of the compounds is based on the position of the metal atom of MX_2 in the periodic table. The missing data points in the plots show the instability of those compounds toward hydrogen adsorption; that is, in these cases hydrogen pulls out the 'X' atom from the monolayer and moves far from the surface. All energies shown in the ordinates are in electronvolts.

DOI: 10.1021/acs.jpclett.5b00353
J. Phys. Chem. Lett. 2015, 6, 1577−1585

evolve hydrogen, and it has been found that the optimum value of the free energy of hydrogen adsorption (ΔG_H) on the surface of the material should be close to zero.[3,8,16] The free energy of hydrogen adsorption comes out as a descriptor based on the Volmer−Heyrovsky route for the HER. The steps involved in the Volmer−Heyrovsky process can be written as[33,34]

$$H^+ + e^- + * \rightarrow H^* \quad (1)$$

$$2H^* \rightarrow H_2 + 2^* \quad (2)$$

where * denotes the active site. At zero potential the free-energy difference between $H^+ + e^-$ and H_2 is (by definition) zero, and the intermediate state of adsorbed hydrogen provides an effective barrier for the process, which should be as close to zero as possible. Therefore, to determine the reactivity of the basal plane, we first calculate the hydrogen adsorption energy on different sites. The adsorption energy is calculated relative to the hydrogen molecule and the most stable clean substrate within the given class (1T or 2H). In all of the 1T and 2H classes of the MX_2 structures, we find that the most favorable hydrogen adsorption site on the basal plane is on top of the chalcogen/oxygen atoms. For distorted structures, depending on the symmetry, H will bind differently to the different chalcogen/oxygen atoms. For further analysis we select the adsorption site with the strongest binding. We start with one-fourth (0.25 ML) of a monolayer of coverage (one hydrogen per four chalcogen/metal atom) and select only the compounds binding hydrogen too strongly ($\Delta H_H^{ads} \geq -0.8$) for higher coverages. Calculations for higher H adsorption coverages reveal massive reconstructions, and the final structures do not belong to any of the structure in the 2H and 1T class; therefore, we choose not to explore the cases of higher coverage any further and focus only on one-fourth of a monolayer of coverage in the current work. To establish the trends in the strength of hydrogen binding, we use the heat of adsorption (total energy differences) and incorporate zero-point energies and entropic effects only in the stage of evaluating the suitability of materials for HER.

Figure 4 shows the calculated heats of hydrogen adsorption (ΔH_{ads}^H) on the 2H and 1T basal planes with 0.25 ML coverage of hydrogen. Upon hydrogen adsorption, not all of the surfaces are stable; therefore, we discard the compounds (missing data points) in the plots that are unstable toward hydrogen adsorption, that is, in these cases hydrogen pulls out the 'X' atom from the monolayer and moves far from the surface or the structure massively reconstructs and transforms to a structure not belonging to the 2H or 1T class. As can be seen, the heat of adsorption varies widely by several electronvolts. An overall trend is that the bonding strength is increased as the electronegativity of the chalcogenide is increased. There is clearly no simple relation between the hydrogen bonding to the 2H and 1T structures. Depending on the metal and chalcogenide in question the bonding to the 1T class may be stronger or weaker than the bonding to the 2H class.

To shed some light on the chemistry behind the different adsorption energies, we shall focus on only two of the metal groups that stand out in Figure 4. For the metals Ti, Zr, and Hf the bonding to the 2H structure is clearly stronger than that for the 1T, while for the metals Cr, Mo, and W we have an opposite trend. To understand these opposite behaviors we analyze the density of states (DOS) projected onto the 'X' p orbital in MX_2.[16] Figure 5a−d shows the DOS of pristine

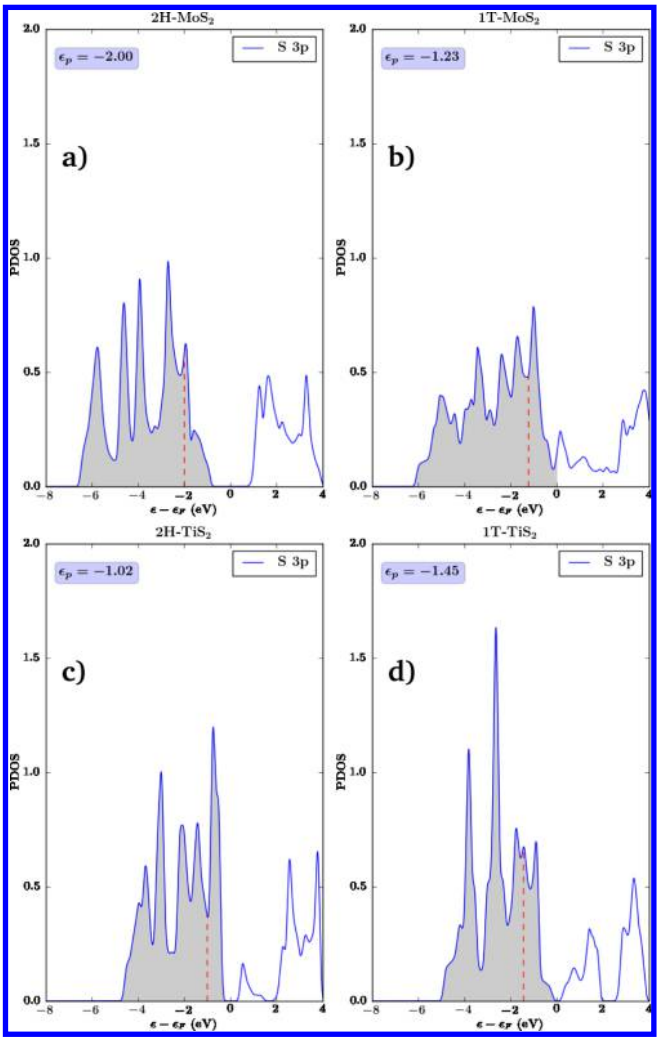

Figure 5. (a) Density of states (DOS) plot of MoS_2 and TiS_2 in the 2H and 1T structures. MoS_2 and TiS_2 belong to two different groups as shown in Figure 4). ϵ_p denotes the position of the center of the p band with respect to the Fermi level. The shaded region corresponds to occupied states.

monolayers. The calculated position of the p-band center (ϵ_p) (obtained as the first moment of the projected density of states) with respect to the Fermi level of the pristine monolayers explains the difference in reactivity of the two groups. A higher-lying p level indicates possible stronger effects of hybridization with the hydrogen s state.[16] The calculated ϵ_p for MoS_2 in the 1T structure lies closer to the Fermi level as compared with the 2H structure, whereas for TiS_2, the ϵ_p for the 2H structure lies closer to the Fermi level as compared with the 1T structure. Table 2 shows the adsorption energy (ΔH_{ads}^H) and center of p band for compounds selected from the groups to which MoS_2 and TiS_2 belong. As can be seen from the Table, other compounds also show the same correlation between ϵ_p and ΔH_{ads}^H. These results show that the nature of the metal atom[35] along with the symmetry of the structure has a significant effect on the reactivity.

We calculate for 0.25 ML coverage the heats of adsorption (ΔH_{ads}^H) including error bars (σ) with the BEEF-vdW functional to assess the confidence interval of heats of adsorption.[22] As mentioned earlier, we add zero point and entropic corrections of 0.32 eV in all the heats of adsorption to get the free energy of adsorption. Here we assume that the corrections will not vary

DOI: 10.1021/acs.jpclett.5b00353
J. Phys. Chem. Lett. 2015, 6, 1577−1585

Table 2. Heat of Adsorption of Hydrogen, ΔH^{H}_{ads}, and the Center of the p Band, ϵ_p, for Compounds Belonging to Different Groups in the 2H and 1T Structures[a]

2H	ϵ_p	ΔH^{H}_{ads}	1T	ϵ_p	ΔH^{H}_{ads}
MoS_2	−2.00	1.68 ± 0.07	MoS_2	−1.23	0.10 ± 0.13
$MoSe_2$	−1.74	1.82 ± 0.13	$MoSe_2$	−1.46	0.64 ± 0.11
WS_2	−2.32	1.95 ± 0.08	WS_2	−1.37	0.23 ± 0.14
WSe_2	−2.03	2.03 ± 0.14	WSe_2	−1.29	0.78 ± 0.15
TiS_2	−1.02	−0.05 ± 0.13	TiS_2	−1.45	0.40 ± 0.09
$TiSe_2$	−0.89	0.44 ± 0.12	$TiSe_2$	−1.38	0.90 ± 0.10
ZrS_2	−0.96	0.11 ± 0.10	ZrS_2	−1.42	0.94 ± 0.07
$ZrSe_2$	−0.80	0.51 ± 0.10	$ZrSe_2$	−1.34	1.19 ± 0.09

[a]Grouping of the compounds is performed based on the group of the periodic table to which the metal atom in MX_2 belongs.

much for different compounds, hence we choose the same correction as we have calculated for 1T-MoS_2 monolayer structure. Since the optimum value of free energy (ΔG^{opt}) for HER is ∼0.0 eV, we consider the range of free energy from −0.5 to 0.5 eV to take into account the effect of coverage, strain, and so on.[8,36] Having an allowable range of free energy, mean adsorption energies along with uncertainties allows us to calculate the probability ($P(|\Delta G| \leq 0.5)$) of a material having free energy for HER in the given interval. Assuming a Gaussian distribution of uncertainties around the mean value, $\bar{E}$, of the adsorption, probabilities can be calculated as

$$P(|\Delta G| \leq 0.5) = \frac{1}{\sqrt{2\pi\sigma^2}} \int_{-0.5-\bar{E}}^{0.5+\bar{E}} \exp\left(-\frac{E^2}{2\sigma^2}\right) dE \quad (3)$$

The calculated probabilities will help in narrowing down the material space for potential experimental investigation by discarding the materials with very small probabilities. In Figure 6, we show the compounds in the 2H and 1T class of structures ranked according to the calculated probability measure. The Figure includes compounds with a probability as low as 0.15. This leads to 21 compounds in the 2H class of structures and 26 compounds in the 1T class of structures. For each compound, the calculated free energy is shown together with the error bar from the BEEF−vdW ensemble. We see that MoS_2 and WS_2 appear on the list of candidates for the 1T structure (although not with the highest probability) in support of the recent experiments indicating possible hydrogen evolution for these systems.[8,10] The only compounds that appear on both the 2H and 1T lists are NbS_2, RhS_2, RuS_2, IrS_2, CoS_2, $ScSe_2$, RuO_2, and $TaTe_2$, illustrating the fact that the chemical activity is very sensitive to the crystal structure.

Having identified possible 2D materials with promising binding properties for hydrogen, it is appropriate to investigate the stability of these materials further. There are two possibilities that may hamper the growth and stability of the 2H or 1T phases of the 2D materials found to be active for HER: (1) much higher stability of the competing bulk structures or the standard states, thus leading to the dissociation of the 2D phase into these compounds, and (2) relative stability of the 2H and 1T phases also matters. For example, if the 2H phase of a material is HER-active but is much higher in energy than the 1T structure, it is unlikely that the material can be synthesized and stabilized in the 2H structure. Therefore, the HER-active 2D materials must not lie above a certain degree of metastability with respect to the competing bulk structures or the standard states, and also it should not be energetically too high with respect to the other 2D phase of the material. In the present work, we do not explore the stability of compounds in water because a recent study has shown that with stabilizing agents compounds can be stabilized in water, making this criterion less important.[37] The presence of water might also have an effect on the adsorption energies, but in the current work having a fairly wide window of the free energy of adsorption for the candidate materials, we expect to have allowed for the effect of water.

Calculated data to address the previously described issues are collected in Table 3a,b. The second column of the Table shows the calculated standard heats of formation, ΔH, for the monolayers (as shown for all the compounds in Figure 2) in the 2H and 1T classes of structure, respectively. The third column ΔH_{hull} is calculated using structural information from the OQMD database.[38] The OQMD database contains standard DFT energy calculations for a large selection of known compounds from the ICSD database[39] plus a number of standard structures. In the case of binary systems, this results in

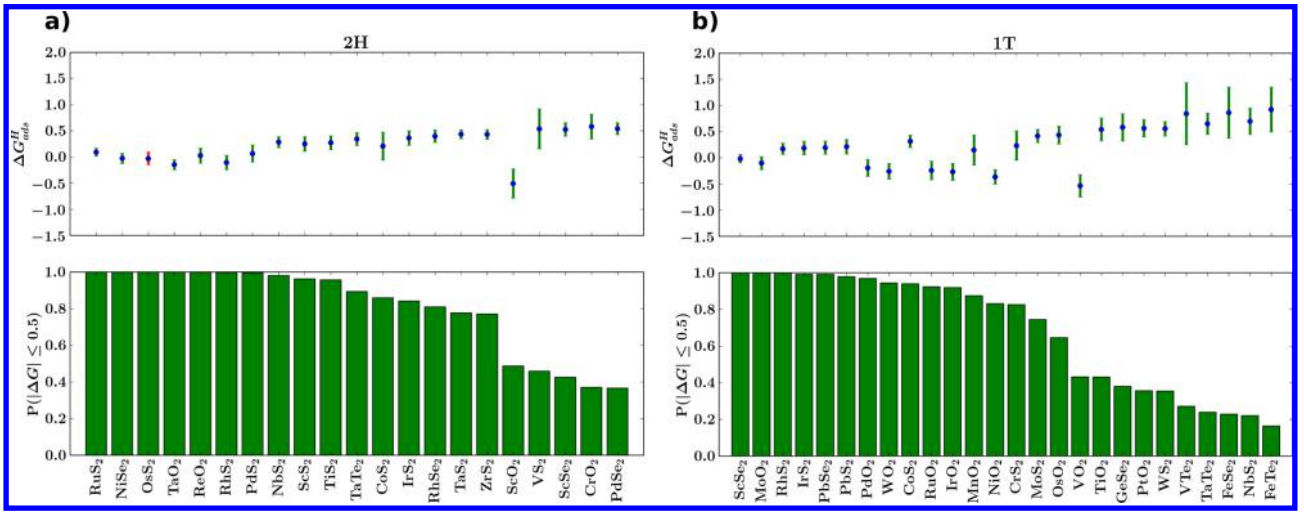

Figure 6. (a) 2H compounds having a free energy of hydrogen adsorption (ΔG^{H}_{ads}) in the range of (−0.5, 0.5) eV along with uncertainties for 0.25 ML coverage and probabilities ($P(|\Delta G| \leq 0.5)$) as calculated from eq 3. Red error bars indicate that the structure is unstable with respect to the standard states.

DOI: 10.1021/acs.jpclett.5b00353
J. Phys. Chem. Lett. 2015, 6, 1577−1585

Table 3. (a) Relevant Energies for Analysis of the Stabilities of the Obtained HER Candidates in the 2H-Derived Structures[a] and (b) Similar Table for the 1T Candidates[b]

(a)

2H-MX_2	ΔH	ΔH_{hull}	ΔH_{hull}	$\Delta H_{expt.}$	ref 40	$\Delta H_{2H/1T}$	$P(\lvert\Delta G\rvert \leq 0.5)$
RuS_2	−0.31	−0.70	0.39	−0.71	no	−0.01	1.00
$NiSe_2$	−0.21	−0.34	0.13	−0.38	no	0.17	1.00
OsS_2	0.34	−0.60	0.94	NA	no	−0.01	1.00
TaO_2	−2.58	−3.00	0.42	NA	no	−0.07	1.00
ReO_2	−0.91	−1.42	0.51	−1.52	no	0.05	1.00
RhS_2	−0.11	−0.48	0.37	NA	no	0.07	1.00
PdS_2	0.01	−0.31	0.32	−0.28	yes	0.17	1.00
NbS_2	−1.21	−1.20	−0.01	NA	yes	−0.04	0.98
ScS_2	−1.46	−1.46	0.00	NA	no	−0.06	0.96
TiS_2	−1.23	−1.37	0.14	−1.41	yes	0.15	0.96
$TaTe_2$	−0.32	−0.45	0.13	NA	yes	0.00	0.89
CoS_2	−0.33	−0.48	0.15	−0.51	no	0.01	0.86
IrS_2	−0.11	−0.48	0.37	−0.46	no	0.22	0.84
$RhSe_2$	−0.17	−0.45	0.28	NA	no	0.07	0.81
TaS_2	−1.24	−1.22	−0.02	−1.22	yes	−0.02	0.78
ZrS_2	−1.55	−1.73	0.18	−1.99	yes	0.19	0.77
ScO_2	−2.74	−3.17*	0.43	NA	no	0.05	0.49
VS_2	−1.16	−1.14	−0.02	NA	no	−0.02	0.46
$ScSe_2$	−1.30	−1.25*	−0.05	NA	no	−0.01	0.43
CrO_2	−1.99	−2.15	0.16	−2.01	no	0.03	0.37
$PdSe_2$	−0.02	−0.33	0.31	NA	yes	0.22	0.37

(b)

1T-MX_2	ΔH	ΔH_{hull}	ΔH_{hull}	$\Delta H_{expt.}$	ref 40	$\Delta H_{1T/2H}$	$P(\lvert\Delta G\rvert \leq 0.5)$
$ScSe_2$	−1.34	−1.25*	−0.09	NA	no	0.01	1.00
MoO_2	−1.79	−1.95	0.16	−2.04	no	0.31	1.00
RhS_2	−0.32	−0.48	0.16	NA	no	−0.07	1.00
IrS_2	−0.30	−0.48	0.18	−0.46	no	−0.22	0.99
$PbSe_2$	0.04	−0.31*	0.35	NA	no	−0.22	0.99
PbS_2	0.03	−0.32*	0.35	NA	no	−0.28	0.98
PdO_2	−0.48	−0.41	−0.07	NA	no	NA	0.97
WO_2	−1.61	−1.89	0.28	NA	no	0.24	0.94
CoS_2	−0.34	−0.48	0.14	−0.51	no	−0.01	0.94
RuO_2	−0.71	−0.94	0.23	−1.05	no	−0.20	0.92
IrO_2	−0.70	−0.94	0.24	−0.86	no	NA	0.92
MnO_2	−2.00	−1.98	−0.02	−1.80	no	−0.43	0.87
NiO_2	−1.01	−0.79*	−0.22	NA	no	NA	0.83
CrS_2	−0.77	−0.71	−0.06	NA	yes	0.12	0.83
MoS_2	−0.66	−0.93	0.27	−0.95	yes	0.28	0.74
OsO_2	−0.23	−1.10	0.87	−1.02	no	NA	0.65
VO_2	−2.47	−2.63	0.16	−2.48	no	−0.10	0.43
TiO_2	−3.10	−3.29	0.19	−3.26	no	−1.11	0.43
$GeSe_2$	−0.27	−0.34	0.07	−0.39	no	NA	0.38
PtO_2	−0.61	−0.62	0.01	NA	no	NA	0.36
WS_2	−0.59	−0.78	0.19	−0.90	yes	0.18	0.35
VTe_2	−0.40	−0.45	0.05	NA	yes	0.00	0.27
$TaTe_2$	−0.32	−0.45	0.13	NA	yes	0.00	0.24
$FeSe_2$	−0.48	−0.56	0.08	NA	no	−0.05	0.23
NbS_2	−1.18	−1.20	0.02	NA	yes	0.04	0.22
$FeTe_2$	−0.11	−0.20	0.09	−0.25	no	−0.02	0.16

[a] ΔH denotes the calculated standard heat of formation. ΔH_{hull} denotes the heat of formation of the most stable compound (i.e., at the convex hull) in the OQMD database.[38] The symbol * in superscript corresponds to the situation, where no bulk structure with the compound composition lies on the convex hull according to the database. In that case, ΔH_{hull} is calculated as a linear combination of several structures. ΔH_{hull} denotes the difference between the two previous columns; that is, it shows how much the 2D compound lies above or below the convex hull. $\Delta H_{expt.}$ indicates the experimental standard heats of formation as listed in the OQMD database. Lebègue al.[40] have analyzed the possibilities for forming 2D compounds based on the layered character of the bulk structures and their result is also listed in the Table. $\Delta H_{2H/1T}$ is the difference between the energies in the two (possibly distorted) 2H and 1T structures. Finally, $P(\lvert\Delta G\rvert \leq 0.5)$ is the probability that the free energy of hydrogen adsorption lies within 0.5 eV from zero, as described in Figure 6. All the energies are in eV/atom. [b] NA in the seventh column indicates that due to massive reconstructions the compound is discarded from the 2H class. All energies are in eV/atom.

DOI: 10.1021/acs.jpclett.5b00353
J. Phys. Chem. Lett. 2015, 6, 1577−1585

calculations of the most stable structures as a function of relative concentration of the two constituents identifying the so-called convex hull of lowest energy structures. For a given MX_2 compound, we extract the structure with the lowest energy at this 1:2 composition of the M-X phase diagram from the database. In most cases a compound with the 1:2 composition exists as the most stable one. If that is not the case we extract the two structures that linearly combine to give the lowest energy of the convex energy hull at the 1:2 composition. We note that all structures are reoptimized and energies are calculated with the approach we use here. The fourth column, ΔH_{hull}, shows our calculated heat of formation with respect to the convex hull. If two structures are used to obtain the energy of the hull, ΔH_{hull}, then it is indicated with an asterisk on the number. For comparison, the experimental heats of formation for the most stable compounds are shown in the third column when available in the OQMD database. As can be seen, the calculated heats of formation are in good agreement with the experimental data with a RMS deviation of only 0.09 eV. The fourth column shows the difference between columns 1 and 2, that is, how much the energy of the 2D material is above (or below) the energy at the convex hull. The seventh column in Table 3 shows the heat of formation of the 2H (1T) class of structure with respect to the 1T (2H) class of structures $\Delta H_{2H/1T}$ ($\Delta H_{1T/2H}$). We find that the energy difference between the catalytically active candidate and its analogue in the other structure is usually not very large. As previously mentioned HER-active materials like MoS_2 and WS_2 in the 1T phase have a degree of metastability as high as 0.3 eV/atom with respect to the 2H phase and lie above the hull by ∼0.3 eV/atom; nevertheless, they have been synthesized and stabilized under ambient conditions.[10] Surprisingly, none of the other HER-active materials differ from their corresponding 2D analogue in energy by >0.3 eV/atom. Therefore, in the list of proposed HER materials, if the material can be synthesized and stabilized in one of the two phases, then it is highly likely that it can be synthesized and stabilized in the other phase as well.

Some of the compounds like PdS_2 and $PdTe_2$, which have been found to be HER-active in the current work, have also been suggested to exist in monolayer form by Lebègue al.[40] As can be seen from Table 3a,b, PdS_2 and $PdTe_2$ lie above the hull by ∼0.35 eV. Therefore, we choose a threshold of 0.4 eV for ΔH_{hull} for stability of compounds. The given criteria narrows the list of the candidates, specifically OsS_2, ReO_2, $OsSe_2$, ScO_2, and RuO_2 in the 2H class of candidates and OsO_2 in the 1T class of candidates do not fulfill this criteria. The names of these compounds are italicized in Table 3a,b. A few monolayers in Table 3a,b have lower energy than the energy of the convex hull. One of the reasons for this behavior might be the existence of other more stable bulk structures than the ones considered in the OQMD database, for example, structures obtained by stacking the 2D layers.

Additionally, we also compare our findings of 2D materials for HER with the recent study by Lebègue et al.[40] that is based on predicting the existence of 2D materials from experimental bulk structures. The exiguous overlap between our results and the ones by Lebègue al. arises from the fact that our conclusions are based on thermodynamic arguments obtained with ab initio calculations, whereas the work of Lebègue al. relies more on heuristic arguments of the ability of cleaving a bulk along a direction of weak bonding. The compounds of the MX_2 class proposed in their work are all present in our work, thus supporting our approach. A few compounds in Table 3a,b are written in bold. We select them based on the work by Lebègue et al.[40] by looking for "yes" in the column VI in Table 3a,b because it is highly likely that they can be synthesized and stabilized with minimal effort.

In the current study, we suggest several 2D materials in the 2H and 1T structures as potential candidates for the hydrogen evolution reaction. The activity of the basal plane in all of the discovered candidates will provide a much larger number of active sites as compared with 2D materials like 2H MoS_2, where only edges are active. Our analysis is using the calculated adsorption free energy as a well-established descriptor for hydrogen evolution. We furthermore investigate the stability of the compounds in some detail by comparing heats of formation of both competing layered phases and bulk structures. Recent experimental stabilization of different layered phases seem to indicate that fairly large metastability of several tenths of an eV/atom can be overcome by appropriate synthesis routes, making it likely that many of the suggested compounds could be experimentally synthesized. It has recently been demonstrated that the MoS_2 and WS_2 in the 1T phase can evolve hydrogen, and these systems also appear in our screening, but other identified systems should according to the calculations provide higher activity. The calculations therefore invite further investigation of some of the best candidates suggested here.

■ ASSOCIATED CONTENT

Ⓢ Supporting Information

Lattice constants and adsorption energy of hydrogen are provided in the tables. This material is available free of charge via the Internet at http://pubs.acs.org.

■ AUTHOR INFORMATION

Corresponding Author

*E-mail: kwj@fysik.dtu.dk.

Notes

The authors declare no competing financial interest.

■ ACKNOWLEDGMENTS

We acknowledge CASE (Catalysis for Sustainable Energy) initiative of the Danish Ministry of Science for funding the project. The Center for Nanostructured Graphene is sponsored by the Danish National Research Foundation, Project DNRF58. We thank Jens K. Nørskov and Charlie Tsai from SUNCAT (Stanford University) for helpful discussions.

■ REFERENCES

(1) Dresselhaus, M. S.; Thomas, I. L. Alternative Energy Technologies. *Nature* **2001**, *414*, 332−337.

(2) Crabtree, G. W.; Dresselhaus, M. S.; Buchanan, M. V. The Hydrogen Economy. *Phys. Today* **2004**, *57*, 39−44.

(3) Greeley, J.; Jaramillo, T. F.; Bonde, J. L.; Chorkendorff, I.; Nørskov, J. K. Computational High-Throughput Screening of Electrocatalytic Materials for Hydrogen Evolution. *Nat. Mater.* **2006**, *5*, 909−913.

(4) Okamoto, Y.; Ida, S.; Hyodo, J.; Hagiwara, H.; Ishihara, T. J. Synthesis and Photocatalytic Activity of Rhodium-doped Calcium Niobate Nanosheets for Hydrogen Production from a Water/Methanol System without Cocatalyst Loading. *J. Am. Chem. Soc.* **2011**, *133*, 18034−18037.

(5) Cobo, S.; Heidkamp, J.; Jacques, P.-A.; Fize, J.; Fourmond, V.; Guetaz, L.; Jousselme, B.; Ivanova, V.; Dau, H.; Palacin, S.; et al. A Janus Cobalt-Based Catalytic Material for Electro-Splitting of Water. *Nat. Mater.* **2012**, *11*, 802−807.

DOI: 10.1021/acs.jpclett.5b00353
J. Phys. Chem. Lett. 2015, 6, 1577−1585

(6) Liu, P.; Rodriguez, J. A. Catalysts for Hydrogen Evolution from the [NiFe] Hydrogenase to the Ni_2P (001) Surface: The Importance of Ensemble Effect. *J. Am. Chem. Soc.* **2005**, *127*, 14871−14878.
(7) Popczun, E. J.; McKone, J. R.; Read, C. G.; Biacchi, A. J.; Wiltrout, A. M.; Lewis, N. S.; Schaak, R. E. Nanostructured Nickel Phosphide as an Electrocatalyst for the Hydrogen Evolution Reaction. *J. Am. Chem. Soc.* **2013**, *135*, 9267−9270.
(8) Voiry, D.; Yamaguchi, H.; Li, J.; Silva, R.; Alves, D. C. B.; Fujita, T.; Chen, M.; Asefa, T.; Shenoy, V. B.; Eda, G.; et al. Enhanced Catalytic Activity in Strained Chemically Exfoliated WS_2 Nanosheets for Hydrogen Evolution. *Nat. Mater.* **2013**, *12*, 850−855.
(9) Lukowski, M. A.; Daniel, A. S.; Meng, F.; Forticaux, A.; Li, L.; Jin, S. Enhanced Hydrogen Evolution Catalysis from Chemically Exfoliated Metallic MoS_2 Nanosheets. *J. Am. Chem. Soc.* **2013**, *135*, 10274−10277.
(10) Voiry, D.; Salehi, M.; Silva, R.; Fujita, T.; Chen, M.; Asefa, T.; Shenoy, V. B.; Eda, G.; Chhowalla, M. Conducting MoS_2 Nanosheets as Catalysts for Hydrogen Evolution Reaction. *Nano Lett.* **2013**, *13*, 6222−6227.
(11) Wang, H.; Lu, Z.; Kong, D.; Sun, J.; Hymel, T. M.; Cui, Y. Electrochemical Tuning of MoS_2 Nanoparticles on Three-dimensional Substrate for Efficient Hydrogen Evolution. *ACS Nano* **2014**, *8*, 4940−4947.
(12) Jaramillo, T. F.; Jørgensen, K. P.; Bonde, J.; Nielsen, J. H.; Horch, S.; Chorkendorff, I. Identification of Active Edge Sites for Electrochemical H_2 Evolution from MoS_2 Nanocatalysts. *Science* **2007**, *317*, 100−102.
(13) Enyashin, A. N.; Yadgarov, L.; Houben, L.; Popov, I.; Weidenbach, M.; Tenne, R.; Bar-Sadan, M.; Seifert, G. New Route for Stabilization of 1T-WS_2 and MoS_2 Phases. *J. Phys. Chem. C* **2011**, *115*, 24586−24591.
(14) Bollinger, M. V.; Jacobsen, K. W.; Nørskov, J. K. Atomic and Electronic Structure of MoS_2 Nanoparticles. *Phys. Rev. B* **2003**, *67*, 085410.
(15) Hinnemann, B.; Moses, P. G.; Bonde, J.; Jørgensen, K. P.; Nielsen, J. H.; Horsch, S.; Chorkendorff, I.; Nørskov, J. K. Biomemetic Hydrogen Evolution: MoS_2 Nanoparticles as Catalyst for Hydrogen Evolution. *J. Am. Chem. Soc.* **2005**, *127*, 5308−5309.
(16) Tsai, C.; A.-Pedersen, F.; Nørskov, J. K. Tuning the MoS_2 Edge-Site Activity for Hydrogen Evolution via Support Interactions. *Nano Lett.* **2014**, *14*, 1381−1387.
(17) Enkovaara, J.; Rostgaard, C.; Mortensen, J. J.; Chen, J.; Dulak, M.; Ferrighi, L.; Gavnholt, J.; Glinsvad, C.; Haikola, V.; Hansen, H. A.; et al. Electronic Structure Calculations with GPAW: A real-space Implementation of the Projector Augmented-wave Method. *J. Phys.: Condens. Matter* **2010**, *22*, 253202.
(18) Kresse, G.; Joubert, D. From Ultrasoft Pseudopotentials to the Projector Augmented-Wave Method. *Phys. Rev. B* **1999**, *59*, 1758−1775.
(19) Perdew, J. P.; Burke, K.; Ernzerhof, M. Generalized Gradient Approximation Made Simple. *Phys. Rev. Lett.* **1996**, *77*, 3865.
(20) Stevanovic, V.; Lany, S.; Zhang, X.; Zunger, A. Correcting Density Functional Ttheory for Accurate Predictions of Compound Enthalpies of Formation: Fitted Elemental-phase Reference Energies. *Phys. Rev. B* **2012**, *85*, 115104.
(21) Monkhorst, H. J.; Pack, J. D. Special Points for Brillouin-zone Integrations. *Phys. Rev. B* **1976**, *13*, 12.
(22) Wellendorff, J.; Lundgaard, K. T.; Møgelhøj, A.; Petzold, V.; Landis, D. D.; Nørskov, J. K.; Bligaard, T.; Jacobsen, K. W. Density Functionals for Surface Science: Exchange-correlation Model Development with Bayesian Error Estimation. *Phys. Rev. B* **2012**, *85*, 235149.
(23) Medford, A. J.; Wellendorff, J.; Vojvodic, A.; Studt, F.; A.-Pedersen, F.; Jacobsen, K. W.; Bligaard, T.; Nørkov, J. K. Assessing the Reliability of Calculated Catalytic Ammonia Synthesis Rates. *Science* **2014**, *345*, 197.
(24) Irikura, K. K. Experimental Vibrational Zero-Point Energies: Diatomic Molecules. *J. Phys. Chem. Ref. Data* **2007**, *36*, 389.
(25) Linstrom, P. J., Mallard, W. *NIST Chemistry WebBook*; NIST Standard Reference Database 69; National Institute of Standards and Technology: Gaithersburg, MD, 1998.
(26) Kan, M.; Wang, J. Y.; Li, X. W.; Zhang, S. H.; Li, Y. W.; Kawazoe, Y.; Sun, Q.; Jena, P. Structures and Phase Transition of a MoS_2 Monolayer. *J. Phys. Chem. C* **2014**, *118*, 1515−1522.
(27) Ataca, C.; ahin, H.; Ciraci, S. Stable, Single-Layer MX_2 Transition-Metal Oxides and Dichalcogenides in a Honeycomb-Like Structure. *J. Phys. Chem. C* **2012**, *116*, 8983−8999.
(28) Lin, Y.-C.; Dumcenco, D. O.; Huang, Y.-S.; Suenaga, K. Atomic Mechanism of the Semiconducting-to-Metallic Phase Transition in Single-Layered MoS_2. *Nat. Nanotechnol.* **2014**, *9*, 391−396.
(29) Stokes, H. T.; Hatch, D. M. FINDSYM: Program for Identifying the Space Group Symmetry of a Crystal. *J. Appl. Crystallogr.* **2005**, *38*, 237−238.
(30) Tongay, S.; Fan, W.; Kang, J.; Park, J.; Koldemir, U.; Suh, J.; Narang, D. S.; Liu, K.; Ji, J.; Li, J.; et al. Monolayer Behaviour in Bulk ReS_2 Due to Electronic and Vibrational Decoupling. *Nat. Commun.* **2014**, *5*, 3252.
(31) Rossnage, K. On the Origin of Charge-Density Waves in Select Layered Transition-Metal Dichalcogenides. *J. Phys.: Condens. Matter* **2011**, *23*, 213001.
(32) Dolui, K.; Sanvito, S. Dimensionality Driven Charge Density Wave Instability in TiS_2. *arXiv* **2013**, arXiv:1310.1866v1 [cond-mat.mes-hall].
(33) Trasatti, S. Work Function, Electronegativity, and Electrochemical Behaviour of Metals: III. Electrolytic Hydrogen Evolution in Acid Solutions. *J. Electroanal. Chem.* **1972**, *39*, 163.
(34) Bockris, J. O.; Reddy, A. K. N.; Gamboa-Aldeco, M. *Modern Electrochemistry 2A*, 2nd ed.; Kluwer Academic/Plenum Publishers: New York, 1998.
(35) (a) Tsai, C.; Chan, K.; Nørskov, J. K.; Abild-Pedersen, F. Understanding the Reactivity of Layered Transition-Metal Sulfides: A Single Electronic Descriptor for Structure and Adsorption. *J. Phys. Chem. Lett.* **2014**, *5*, 3884−3889. (b) Tsai, C.; Chan, K.; Nørskov, J. K.; Abild-Pedersen, F. Theoretical Insights into the Hydrogen Evolution Activity of Layered Transition Metal Dichalcogenides. *Surf. Sci.* **2015**, 10.1016/j.susc.2015.01.019.
(36) Seitz, L. C.; Chen, Z.; Forman, A. J.; Pinaud, B. A.; Benck, J. D.; Jaramillo, T. F. Modeling Practical Performance Limits of Photoelectrochemical Water Splitting Based on the Current State of Materials Research. *ChemSusChem* **2014**, *7*, 1372.
(37) Mubeen, S.; Lee, J.; Singh, N.; Moskovitsb, M.; McFarland, E. W. Stabilizing Inorganic Photoelectrodes for Efficient Solar-to-Chemical Energy Conversion. *Energy Environ. Sci.* **2013**, *6*, 1633.
(38) Saal, J. E.; Kirklin, S.; Aykol, M.; Meredig, B.; Wolverton, C. Materials Design and Discovery with High-Throughput Density Functional Theory: The Open Quantum Materials Database (OQMD). *JOM* **2013**, *65*, 1501−1509.
(39) Belsky, A.; Hellenbrandt, M.; Karen, V. L.; Luksch, P. New developments in the Inorganic Crystal Structure Database (ICSD): Accessibility in Support of Materials Research and Design. *Acta Crystallogr.* **2002**, *B58*, 364−369.
(40) Lebègue, S.; Björkman, T.; Klintenberg, M.; Nieminen, R. M.; Eriksson, O. Two-Dimensional Materials from Data Filtering and Ab Initio Calculations. *Phys. Rev. X* **2013**, *3*, 031002.

DOI: 10.1021/acs.jpclett.5b00353
J. Phys. Chem. Lett. 2015, 6, 1577−1585